THE JOURNAL OF PHYSICAL CHEMISTRY A

 VOLUME 106, NUMBER 8, FEBRUARY 28, 2002

FEATURE ARTICLE

Investigating the Phase-Dependent Reactivity of Chlorine Dioxide Using Resonance Raman Spectroscopy

Philip J. Reid*

Department of Chemistry, University of Washington, Box 351700, Seattle, Washington 98195

Received: September 7, 2001

Recent progress in understanding the phase-dependent reactivity of chlorine dioxide (OClO) is outlined. Specifically, resonance Raman intensity analysis (RRIA) and time-resolved resonance Raman (TRRR) studies of OClO photochemistry in solution are presented. The RRIA studies demonstrate that the optically prepared excited-state undergoes significant modification in solution relative to the gas phase. Specifically, the substantial evolution that occurs along the asymmetric-stretch coordinate in the gas phase is restricted in solution. The absence of substantial evolution along the asymmetric-stretch coordinate results in the preservation of ground-state symmetry in the excited state. The role of symmetry in defining the reaction coordinate and the solvent−solute interactions responsible for modification of the excited-state potential energy surface are discussed. TRRR studies performed with pump and probe wavelengths at 390 nm are presented which demonstrate that geminate recombination of the primary photoproducts resulting in the reformation of ground-state OClO is a central feature of OClO photochemistry in solution. Time-resolved anti-Stokes experiments are also presented which demonstrate that the OClO vibrational−relaxation dynamics are solvent dependent. Finally, TRRR studies performed with pump and probe wavelengths of 390 and 260 nm, respectively, are presented. In these studies, ClOO production and subsequent decay resulting in Cl production on the subnanosecond time scale is observed. The current picture of OClO photochemistry derived from these studies is discussed, and future directions for study are outlined.

Introduction

The suggestion that anthropogenic compounds contribute to the transport and subsequent production of atomic chlorine in the stratosphere has motivated numerous studies of the halogen-based chemistry that results in stratospheric ozone loss.[1−4] These studies have demonstrated that numerous chemical and photochemical processes participate in the uptake and release of atomic chlorine (Cl), a central species responsible for ozone depletion.[5,6] The construction of stratospheric chemical models requires accurate knowledge of the rates and product-formation quantum yields for these processes, and it is currently recognized that these reaction parameters may depend on the environment in which the reaction occurs.[4,7,8] For example, aerosols or polar stratospheric clouds can promote chemistry that is significantly different from that which occurs in the gas phase. Therefore, the current challenge in this area is to not only determine the extent to which a given reaction changes as a function of environment but to also understand the fundamental reasons for this behavior.

Our interest involves the photochemistry of halooxides, and chlorine dioxide (OClO) in particular.[9−13] This compound is of interest because of its participation in many stratospheric photochemical processes and for its role as an indicator of

* To whom correspondence should be addressed. E-mail: preid@chem.washington.edu.

10.1021/jp013491y CCC: $22.00
Published on Web 02/21/2002

stratospheric chlorine activation.[14,15] The following reaction channels are available to OClO following photoexcitation[11]:

$$\mathrm{OClO}\ (\mathrm{X}^2\mathrm{B}_2) \xrightarrow{h\nu} \mathrm{ClO}(^2\Pi) + \mathrm{O}(^3\mathrm{P}_g) \quad (1)$$

$$\mathrm{OClO}\ (\mathrm{X}^2\mathrm{B}_2) \xrightarrow{h\nu} \mathrm{Cl}(^2\mathrm{P}_u) + \mathrm{O}_2\ (^1\Delta_g, {}^3\Sigma_g^-) \quad (2)$$

$$\mathrm{OClO}\ (\mathrm{X}^2\mathrm{B}_2) \xrightarrow{h\nu} \mathrm{ClOO} \xrightarrow{\Delta} \mathrm{Cl}(^2\mathrm{P}_u) + \mathrm{O}_2\ (^3\Sigma_g^-, {}^1\Delta_g) \quad (3)$$

Of relevance to halogen-mediated ozone depletion is the ability of OClO to photochemically produce Cl via reactions ii and iii. The quantum yield for Cl production (Φ_{Cl}) is dependent on phase, with $\Phi_{Cl} \leq 0.04$ in the gas phase and increasing to unity in low-temperature matrixes.[11,16−36] Aqueous OClO demonstrates intermediate behavior with $\Phi_{Cl} = 0.1$.[37−43] In addition, Cl production is a bifurcated process in solution, with reactions ii and iii contributing 80% and 20% to Φ_{Cl}, respectively.[44,45] The substantial increase in Φ_{Cl} in condensed environments lead to the suggestion that this compound may make a significant contribution to stratospheric ozone depletion.[9,11] However, studies of model PSCs suggest that equilibrium concentrations of OClO on such surfaces are modest thereby offsetting any increase in Φ_{Cl}. As such, the impact of OClO photochemistry on stratospheric Cl concentrations is expected to be modest.[46,47] However, the phase dependence of Φ_{Cl} makes this compound an excellent case in which to investigate solvent-dependent photochemical reactivity in an environmental context.

In our attempts to understand the fundamental aspects behind the phase-dependent reactivity of OClO, we have employed a multidimensional experimental approach that utilizes three spectroscopic techniques: resonance Raman intensity analysis (RRIA), time-resolved resonance Raman (TRRR), and femtosecond pump−probe (FPP) spectroscopy. The synergistic application of these techniques allows for the study of photochemical reactivity from the initial excited-state evolution to the appearance and relaxation of the ground-state products. In this manuscript, we summarize the major findings from our studies and discuss how these results have refined our understanding of the phase-dependent reactivity of OClO. Our work can be partitioned into studies that explore the excited-state dynamics of OClO and studies in which the production and relaxation of the ground-state photoproducts are investigated. Therefore, this paper is partitioned accordingly. Although the focus of this manuscript is on the photochemistry of OClO, the questions addressed here are common to many reactions of environmental importance. As such, this work represents not only an attempt to understand OClO photochemistry but also the development of an experimental methodology applicable to a wide range of environmental processes.

Excited-State Reaction Dynamics of OClO

Background. Early spectroscopic studies of OClO focused on its electronic absorption spectrum and, in particular, the transition centered at ∼360 nm (Figure 1A).[48,49] This feature was assigned as the $^2B_1$ (ground) to $^2A_2$ (excited) transition corresponding to the advancement of an electron from an orbital of a_2 symmetry to one of b_1 symmetry.[50] This change in electronic structure weakens the Cl−O bond and decreases the antibonding character between the terminal oxygen atoms. Consequently, the transition exhibits significant vibronic structure involving the symmetric-stretch and bend coordinates. In addition, substantial intensity is observed for even-overtone transitions involving the asymmetric-stretch coordinate (Figure 1B). The ground-state symmetry of OClO is C_{2v} such that fundamental intensity involving the asymmetric stretch is not predicted by symmetry. However, differences in the curvature of the excited-state potential energy surface relative to the ground state can give rise to overtone intensity along this coordinate;[51] therefore, the presence of transitions containing asymmetric-stretch overtone intensity demonstrates that the ground and excited potential energy surfaces are substantially different along this coordinate. The origin of this intensity was first assigned to the presence of a double-minimum potential in the excited state.[48,49] Support for this hypothesis was provided by an elegant gas-phase absorption study of OClO seeded into a supersonic jet.[52,53] In this study, the intensity ratio of transitions involving the symmetric stretch to transitions involving the symmetric and asymmetric stretch (e.g., (8,0,0) versus (8,0,2) in Figure 1B) was reproduced using a double-minimum potential. However, alternatives to this model have been presented. Brand and co-workers proposed that anharmonic coupling between the symmetric- and asymmetric-stretch coordinates was responsible for intensity of transitions involving the asymmetric stretch.[54] Recent computational studies have provided substantial support for this model.[55−58] Consensus as to the nature of the $^2A_2$ surface along the asymmetric stretch has yet to be reached; however, both models predict that for gaseous OClO substantial evolution occurs along the asymmetric-stretch coordinate following photoexcitation.

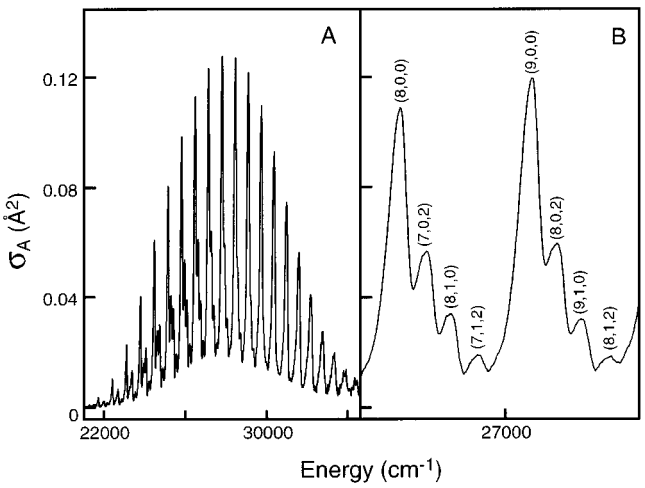

Figure 1. (A) Electronic absorption spectrum of chlorine dioxide vapor. Spectra were obtained at a temperature of 293 K. **(**B**)** Expanded view of the absorption spectrum. Transitions are labeled as (n_1, n_2, n_3) where n is the number of quanta in the excited state along the symmetric stretch (1), bend (2), and asymmetric stretch (3) coordinates.

We have used absolute RRIA to study the structural-relaxation dynamics of OClO that occur following photoexcitation.[59−63] Numerous reviews are available which discuss the details of this technique; therefore, only a brief description is presented here.[64−66] In our studies, absolute Raman scattering cross sections are measured as a function of excitation wavelength, and this information is used in conjunction with the electronic absorption spectrum to develop a model of the optically prepared excited state. Once determined, this model defines the structural relaxation that occurs upon photoexcitation. The connection between excited-state structural evolution and resonance Raman/absorption cross sections was illustrated by Heller and coworkers using their time-dependent formalism, where the

equations that link the Raman (σ_R) and absorption (σ_A) cross sections to excited-state structural evolution are as follows:[67,68]

$$\sigma_R(E_l) = \frac{8\pi E_s^3 E_l e^4 M_{eg}^4}{9\hbar^6 c^4}\int_{-\infty}^{\infty} \partial E_{00}\, H(E_{00})\left|\int_0^{\infty}\langle f|i(t)\rangle e^{i(E_l+E_i)t/\hbar} D(t)\, dt\right|^2 \quad (4)$$

$$\sigma_A(E_l) = \frac{4\pi e^2 E_l M_{eg}^2}{6\hbar^2 cn}\int_{-\infty}^{\infty}\partial E_{00} H(E_{00})\int_{-\infty}^{\infty}\langle i|i(t)\rangle e^{i(E_l+E_i)t/\hbar} D(t)\, dt \quad (5)$$

In the above expressions, M_{eg} is the transition length and E_l and E_s are the incident and scattered frequencies, respectively. Also, n is the refractive index of the solvent, E_i is the initial vibrational energy, and E_{00} is the energy difference between the ground and excited electronic states. $H(E_{00})$ represents inhomogeneous broadening corresponding to the distribution of E_{00} energies created by differing solvent environments that are static on the time scale of Raman scattering. In our work, this distribution was modeled as having a Gaussian functional form. $D(t)$ is the homogeneous damping function corresponding to both excited-state population decay and solvent-induced pure dephasing.[69] We have found that a Gaussian model for $D(t)$ best reproduces the absorption and resonance Raman cross sections of OClO, a result that will be discussed below. The most important components of the above expressions are the time correlators $\langle f|i(t)\rangle$ and $\langle i|i(t)\rangle$. Resonance Raman intensities are dependent on $\langle f|i(t)\rangle$ which represents the overlap of the final state in the scattering process with the initial state propagating under the influence of the excited-state Hamiltonian. One can envision this term as a time-dependent Franck−Condon (FC) factor that becomes finite because of differences in geometry between the ground and excited state. Therefore, the observation of Raman intensity on resonance is evidence that excited-state structural evolution occurs along the corresponding normal coordinate. In analogous fashion, absorption intensity is related to $\langle i|i(t)\rangle$ and corresponds to the time-dependent overlap of the initial ground state with the propagating state. Because the resonance Raman and absorption cross sections both depend on $|i(t)\rangle$, these spectroscopies can be used in tandem to develop a self-consistent, mode-specific description of the excited-state potential energy surface. Furthermore, this analysis can be performed in a variety of environments providing the opportunity to examine the dependence of excited-state curvature on environment.

RRIA of OClO in the Gas and Condensed Phase. The resonance Raman spectrum of OClO dissolved in cyclohexane is presented in Figure 2.[59,60] Significant intensity is observed for transitions involving the symmetric stretch (ν_1) and bend (ν_2) demonstrating that excited-state structural evolution occurs along these coordinates upon photoexcitation. The evolution along these coordinates is quantitatively similar to that which occurs in the gas phase. The most interesting feature of this spectrum is modest intensity at 2190 cm^{-1} corresponding to the asymmetric-stretch overtone transition (Figure 2, middle). This same transition demonstrates substantial intensity in the resonance Raman spectrum of gaseous OClO; therefore, this difference in intensities suggests that the evolution along the asymmetric stretch is significantly restricted in solution.[62] RRIA studies were also performed on OClO dissolved in water and chloroform.[61,63] Figure 2 presents the overtone region for aqueous OClO and demonstrates that essentially no intensity is observed for the asymmetric-stretch overtone transition consistent with the absence of structural evolution along this coordinate. The differences in excited-state relaxation between the gas and solution phase were quantitatively explored by comparing the measured cross sections for asymmetric-stretch overtone transition to those predicted by either the double-well or ab initio model described above. We found that both gas-phase surfaces predict substantially greater intensity than what is observed; therefore, neither gas-phase surface provides an accurate description of the $^2A_2$ state in solution. Instead, the limited asymmetric-stretch overtone intensity was found to be consistent with a modest reduction in frequency from 1100 cm^{-1} in the ground state to ~850 cm^{-1} in the excited state demonstrating that the substantial evolution that occurs along this coordinate in the gas phase is significantly reduced in solution.

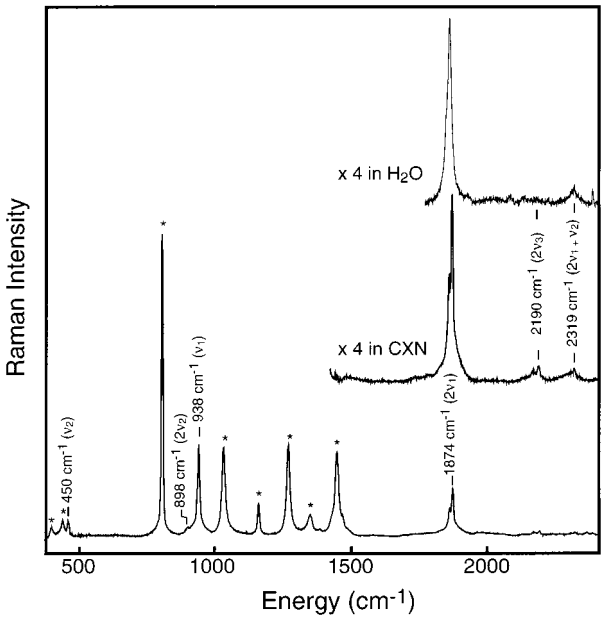

Figure 2. Resonance Raman spectra of OClO dissolved in cyclohexane and water. The bottom spectrum is that of OClO dissolved in cyclohexane. Transitions corresponding to the symmetric stretch (ν_1) and bend (ν_2) are indicated. The middle spectrum is an expanded view of the overtone region, demonstrating the weak intensity of the asymmetric-stretch overtone transition (ν_3). The upper spectrum is the same region for OClO dissolved in water. Scattering corresponding to the asymmetric stretch is not observed. Peaks marked with an asterisk are due to the solvent.

Role of Symmetry in OClO Photochemistry. Through analysis of the gas- and solution-phase absorption and resonance Raman cross sections, a detailed description of the excited-state structural evolution that occurs following OClO photoexcitation has been developed. Figure 3 presents contour plots of the $^2A_2$ surface derived from the computational studies of Peterson and Werner (Figure 3A),[56,57] and from the RRIA of aqueous OClO (Figure 3B).[61] In both environments, significant excited-state structural evolution occurs along the symmetric-stretch and bend coordinates. Evolution along the symmetric stretch is depicted as motion along Q_1, and motion along the bend has been suppressed for clarity. Inspection of the figure demonstrates that the major difference in structural evolution involves the asymmetric-stretch coordinate (Q_3). The ab initio surface predicts that this coordinate undergoes a significant reduction in frequency from 1100 cm^{-1} in the ground state to 419 cm^{-1} in the excited state. Furthermore, this coordinate is anharmonically coupled to the symmetric-stretch coordinate. These effects conspire to provide for significant structural relaxation away

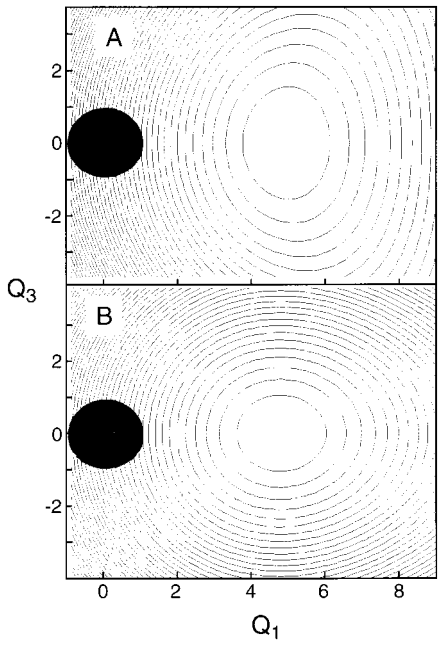

Figure 3. Contour plots of the optically prepared $^2A_2$ surface along the symmetric (Q_1) and asymmetric-stretch coordinates (Q_3) in dimensionless units corresponding to the **(**A**)** ab initio surface[56,57] and (B**)** the solution-phase surface determined by resonance Raman intensity analysis.[59] Contour lines are shown every 500 cm^{-1}. The gray circle represents the first 500 cm^{-1} contour for the ground state corresponding to the optically accessed region of the $^2A_2$ surface.

from $Q_3 = 0$ resulting in a reduction in molecular symmetry from C_{2v} to C_s. Similar behavior is predicted using the double-well model. The surface defined by RRIA (Figure 3B) is substantially steeper along Q_3 such that evolution away from $Q_3 = 0$ is less probable. This restricted evolution results in the preservation of C_{2v} symmetry in the excited state.

We have proposed that the preservation of C_{2v} symmetry in the excited state is one reason for the increase in Φ_{Cl} in solution. Ab initio calculations have indicated that the reduction of symmetry from C_{2v} to C_s serves to reduce the energy barrier for ClO and O formation such that this pathway becomes most favorable.[56] As such, only for geometries at or near C_{2v} is the production of Cl and O_2 predicted to be appreciable. Experimentally, studies of product formation following gaseous OClO photolysis have shown that the excitation of transitions involving the asymmetric stretch results in roughly a 10-fold reduction in Φ_{Cl} relative to excitation of transitions involving the symmetric-stretch exclusively.[17] That is, evolution along the asymmetric stretch serves to promote ClO bond dissociation in favor of Cl production. Our results suggest that similar dynamics contribute to the modification of Φ_{Cl} in solution.

Our focus has been on the dynamics that occur on the $^2A_2$ surface; however, it is important to keep in mind that the lower energy $^2A_1$ and $^2B_2$ excited states also participate in photoproduct production. The sequence of events in OClO photochemistry is believed to be as follows.[11] Internal conversion from the optically prepared $^2A_2$ surface results in production of the $^2A_1$ state, with subsequent production of the lower-energy $^2B_2$ state occurring through $^2A_1$-state internal conversion. Studies of O_2 emission following photoexcitation of OClO in polar and nonpolar solvents have demonstrated that in polar solvents, the production of Cl is accompanied by the production of O_2 ($^3\Sigma_g^-$).[70] However, in nonpolar solvents O_2 ($^1\Delta_g$) is predominantly formed. Under C_{2v} symmetry, only the $^2B_2$ state correlates with the Cl + O_2 ($^1\Delta_g$) channel. Therefore, the O_2 emission studies suggest that in nonpolar and polar solvents Cl is derived from the $^2B_2$ and $^2A_1$ surfaces, respectively. Given the similarity of the $^2A_2$ surfaces in water and cyclohexane, the RRIA results taken in combination with the O_2 emission results demonstrate that partitioning between the Cl + O_2 channels occurs after decay of the $^2A_2$ surface. The above discussion assumes that C_{2v} symmetry is preserved along the reaction coordinate; however, a reduction in molecular symmetry on either the $^2A_1$ or $^2B_2$ surface would substantially alter this picture. For example, symmetry reduction could result in the production of the peroxy isomer, ClOO, which is expected to undergo facile decay into Cl and O_2. Therefore, information regarding the rates and quantum yields for photoproduct formation is needed to further refine our description of OClO photochemisty (see below).

Solvent Response to OClO Photoexcitation. Using absolute resonance Raman intensities, it is possible to partition spectral broadening into its homogeneous and inhomogeneous contributions.[64,66] In our studies, we have found that the homogeneous line width (Γ) is essentially the same in all solvents studied, having an average value of ~90 cm^{-1} corresponding to a total dephasing time of ~60 fs. The homogeneous line width contains contributions from both excited-state population decay and solvent-induced pure dephasing:[69]

$$\Gamma = \frac{1}{T_2} = \frac{1}{2T_1} + \frac{1}{T^*_2}$$

In the above expression, T_2 is the total dephasing time, T_1 is the excited-state lifetime, and T_2^* is the time scale for solvent-induced pure dephasing. Recent fluorescence cross section measurements and femtosecond pump−probe studies of OClO have established that T_1 is ~200 fs.[63,71] Comparison of this time to the total dephasing time (~60 fs) demonstrates that solvent-induced pure dephasing makes the dominant contribution to the homogeneous line width. Therefore, the solvent invariance of Γ suggests that the solvent dynamics responsible for dephasing occur on the same time scale in all solvents studied to date.

We have proposed that the solvent invariance of Γ reflects the dominance of nonpolar or mechanical solvation in response to OClO photoexcitation. The motivation behind this hypothesis is as follows. Ab initio studies predict that the dipole moment (μ) of OClO changes by only ~0.1 D upon photoexcitation and that the direction of the dipole moment remains relatively unchanged.[57] This small change in solute electronic distribution is expected to result in a modest solvent dielectric response. In contrast, the significant displacement along the symmetric-stretch and bend coordinates results in a substantial geometry change upon photoexcitation. Specifically, the excited-state equilibrium geometry corresponds to an increase in Cl−O bond length of ~0.2 Å and a O−Cl−O bond angle decrease of ~9° relative to the ground state.[61] Therefore, we would expect repulsive solvent−solute interactions to be dramatically affected by this geometry change such that mechanical solvation dynamics make the dominante contribution to the solvent response. In support of this hypothesis, we have shown that the viscoelastic continuum (VC) model of nonpolar solvation outlined by Berg is capable of reproducing the homogeneous line width determined in our RRIA studies.[72−74] In this approach, the solvent is treated as a viscoelastic continuum, with the time scale for the solvent response determined by the compressive and shear moduli that characterize the solvent. A comparison between the experimentally determined $D(t)$ for OClO dissolved in cyclohexane and that predicted using the VC model is presented in Figure 4A.[63] The figure demonstrates that VC theory is capable of reproducing both the time scale and the

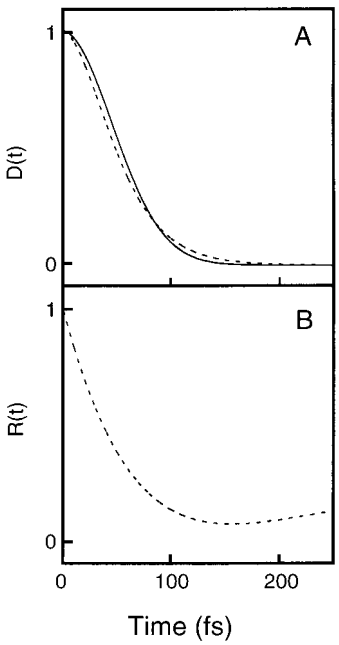

Figure 4. (A) Comparison between the Gaussian functional form for the dephasing ($D(t)$) and the dephasing predicted using viscoelastic continuum theory (VCT). The Gaussian form of $D(t)$ with $\Gamma = 90$ cm^{-1} is given by the solid line and corresponds to the results obtained for OClO dissolved in cyclohexane. The short-dashed line corresponds to $D(t)$ predicted using VCT as described in detail in the literature.[63] (B) The solvent response function predicted using VCT. Parameters used to generate the response function are identical to those used for the corresponding $D(t)$ calculations.

functional form of $D(t)$. The corresponding solvent response function, $R(t)$ (Figure 4B), demonstrates that nonpolar solvation occurs in <100 fs, sufficient to cause dephasing on the ~60 fs time scale. Similar agreement was observed for water and chloroform using representative compressive and sheer moduli for these solvents. Therefore, the agreement between the experimental and VC predicted line widths suggests that nonpolar solvation dynamics are responsible for solvent-induced pure dephasing. Molecular dynamics studies have shown that the repulsive interactions that lead to nonpolar solvation are dominated by a few molecules located in the first solvent shell.[75,76] Clearly, the continuum perspective of the VC model is not capable of describing nonpolar solvation at this level of detail. In collaboration with Oleg Prezhdo (University of Washington), we are performing molecular dynamics studies of OClO dissolved in polar and nonpolar solvents. It is hoped that such studies will provide a microscopic picture of the solvation dynamics operative in solution-phase OClO photochemistry.

One final question concerns the solvent−solute interactions responsible for the restricted evolution along the asymmetric-stretch coordinate. A possible answer to this question is provided by the increase in the inhomogeneous line width with an increase in solvent polarity. Specifically, the standard deviation that characterizes the Gaussian solvent-site distribution increases from 140 cm^{-1} in cyclohexane to 280 cm^{-1} in water. This evolution in inhomogeneous broadening suggests that dielectric solvent−solute interactions are operative on longer time scales (>200 fs) relative to the dynamics responsible for homogeneous broadening. The contribution of dielectric interactions to slower-time solvent dynamics can also be understood by considering the essential invariance of the molecular dipole moment following photoexcitation. This modest change in molecular dipole moment results in an equilibrium solvent configuration for the ground that is the same for the excited state. As such, any change in dipole moment must overcome the stabilization provided by the solvent. Because the largest change in dipole moment occurs with displacement along the asymmetric stretch, it is perhaps not surprising that this coordinate is most affected by the presence of solvent.

OClO Photoproduct Formation Dynamics

Background. As mentioned in the Introduction, two photochemical processes are available to OClO upon photoexcitation, the production of ClO and O or Cl and O_2. Much of the interest in OClO photochemistry has surrounded the mechanism of Cl production, and in determining the quantum yield for this process (Φ_{Cl}). The acquisition of this information for OClO in solution has proven to be quite challenging. Through transient absorption studies with ~100-ps resolution, Simon and coworkers were the first to demonstrate that $\Phi_{Cl} = 0.1$ in aqueous solution.[37,38,77] The optical-density evolution observed in these studies was interpreted in terms of ground-state ClOO production and subsequent decomposition to Cl and O_2.[78] Later transient absorption studies performed with femtosecond time resolution confirmed Φ_{Cl}; however, the mechanism of Cl production was questioned.[39−42,79] Because the dominant photochemical process in solution remains the production of ClO and O, it was suggested that the optical-density evolution was due to the recombination of ClO and O resulting in the production of vibrationally excited ground-state OClO. Differentiation between these models was dependent on studies that could unequivocally determine the identity of those species formed following photoexcitation. With this motivation, we employed time-resolved resonance Raman (TRRR) spectroscopy to study the photoproduct-formation dynamics of solution-phase OClO. This technique provides both kinetic information through the temporal evolution in scattered intensities and structural information characteristic of a vibrational spectroscopy.

Geminate Recombination and Vibrational Relaxation Dynamics. Our first studies involved the photochemistry of aqueous OClO.[80,81] In this work, the temporal evolution in the resonance Raman spectrum following excitation at 390 nm was monitored using a probe wavelength at this same wavelength. The results of this study are summarized in Figure 5A. The spectra presented in the figure are constructed by taking the difference between the probe spectrum in the presence and absence of photolysis. At 0 ps delay, when the pump and probe are overlapped in time, significant depletion in OClO scattering is observed consistent with a reduction in ground-state OClO concentration because of photolysis. As the temporal delay between the pump and probe increases, the OClO depletion intensity decreases up to 20 ps after which time further evolution was not observed out to the longest delays investigated (500 ps). This evolution in depletion intensity demonstrates that ground-state OClO is reformed and directly confirms the geminate recombination model discussed above. Comparison of the depletion at zero delay to the persistent depletion at later delays established that the geminate recombination quantum yield in water is 10.8 ± 0.1.

The kinetics of ground-state OClO reformation by geminate recombination was determined by plotting the intensity of the symmetric-stretch fundamental transition (945 cm^{-1}) as a function of time (Figure 6A). The evolution in intensity was best modeled by a sum of two exponentials having time constants of 0.15 ± 0.1 ps (i.e., instrument-response limited) and 9.2 ± 3.5 ps. A third, long-time component (10 000 ps,

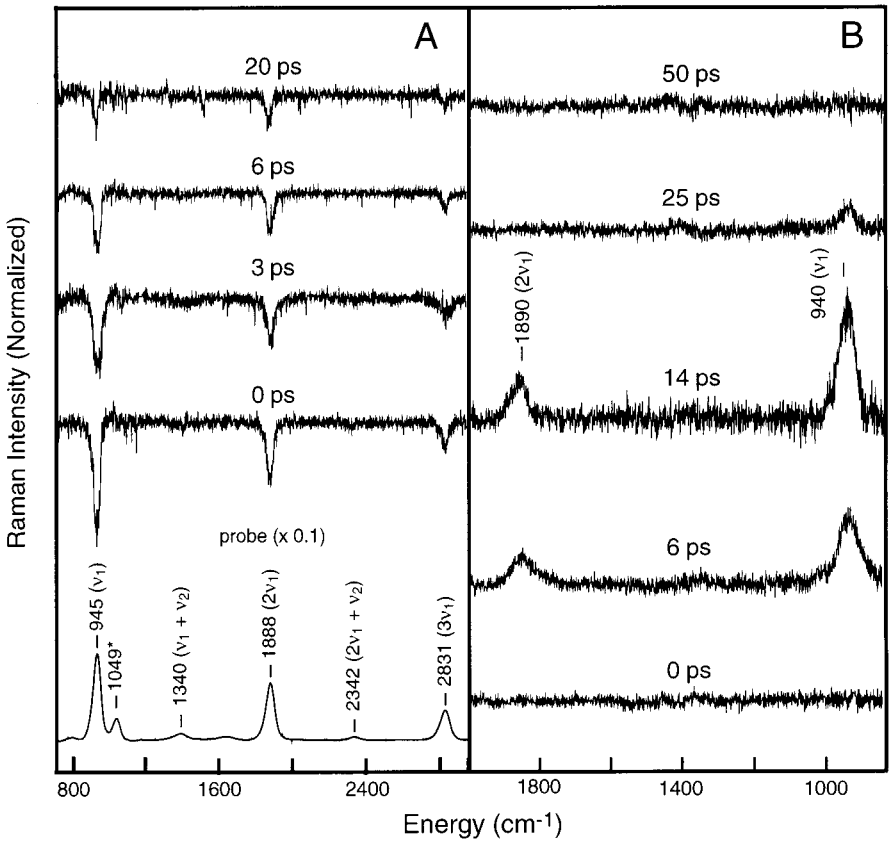

Figure 5. (A) Time-resolved Stokes spectra for aqueous OClO. Spectra were obtained with degenerate pump and probe wavelengths of 390 nm. The 0 ps Stokes spectrum demonstrates depletion in OClO scattering because of photolysis. As the probe is delayed relative to the pump, the depletion amplitude decreases because of OClO reformation via geminate recombination of the ClO and O photoproducts. The peak marked with an asterisk at 1049 cm^{-1} is due to NO_3^- added as an internal scattering standard. (B) Time-resolved anti-Stokes spectra for aqueous OClO. Spectra were obtained with degenerate pump and probe wavelengths of 390 nm. Intensity is observed for the fundamental and overtone transitions of OClO consistent with excess vibrational energy being deposited along this coordinate following geminate recombination.

fixed) was also included in the model to reproduce the persistent depletion in scattering intensity at long delays. These time constants were interpreted as follows. Subpicosecond geminate recombination of the primary ClO and O photofragments results in the production of vibrationally excited OClO which undergoes intermolecular vibrational relaxation on the ~9 ps time scale. Assignment of the early-time depletion recovery to geminate recombination is consistent with the subpicosecond recombination times observed in a variety of other systems.[82] To determine if the 9 ps recovery time constant was indeed due to vibrational relaxation, time-resolved anti-Stokes experiments were performed, with representative results presented in Figure 5B. The figure demonstrates that intensity corresponding to the symmetric-stretch fundamental and overtone transitions is observed. The temporal evolution in symmetric-stretch fundamental anti-Stokes intensity is presented in Figure 6B. Best fit to these data by a sum of two exponentials resulted in the appearance and decay times of 5.2 ± 1.5 and 9.2 ± 1.7 ps, respectively. The agreement between the ~9 ps Stokes appearance and anti-Stokes decay time constants establishes that the intensity evolution that occurs on this time scale is due to vibrational relaxation.

The role of geminate recombination in OClO photochemistry was further explored by performing time-resolved resonance Raman studies in acetonitrile.[81] Studies of I_2^- dissociation have shown that geminate-recombination quantum yields are significantly reduced in acetonitrile relative to water, presumably because of the absence of intermolecular hydrogen bonding in this polar, aprotic solvent.[83] Figure 6C presents the temporal evolution in the OClO symmetric-stretch overtone intensity as a function of time. The evolution observed here is similar to that in water with the extent of depletion decreasing at longer delays. However, the extent of depletion at later times is much greater in acetonitrile compared to water. This observation suggests that the geminate recombination is substantially reduced in this acetonitrile. Consistent with this suggestion, comparison of the initial depletion to that which persists at later delays established that the geminate-recombination quantum yield is reduced to 0.55 ± 0.05 in acetonitrile. Also similar to water, the depletion in OClO scattered intensity undergoes biphasic decay with time-constants of 0.15 ± 0.1 ps (i.e., instrument-response limited) and 33.0 ± 8.1 ps (Figure 6C). Figure 6D presents the anti-Stokes intensity of the symmetric-stretch fundamental transition as a function of time for OClO dissolved in acetonitrile.[81] The figure demonstrates that the appearance and decay of anti-Stokes occurs over a much longer time scale in acetonitrile relative to water demonstrating that the vibrational-relaxation dynamics are solvent dependent. Best fit to the temporal evolution of anti-Stokes intensity in acetonitrile by a sum of two exponentials convolved with the instrument response results in an appearance and decay time-constants of 33.7 ± 4.4 and 36.7 ± 4.6 ps, respectively. The excellent agreement between the later-time Stokes depletion recovery and anti-Stokes decay time constants demonstrates that vibrational relaxation occurs with a time constant of ~35 ps in acetonitrile.

Comparison of the TRRR results for OClO dissolved in water and acetonitrile firmly established that the primary ClO and O photofragments undergo geminate recombination to reform ground-state OClO. Specifically, the recovery of depletion

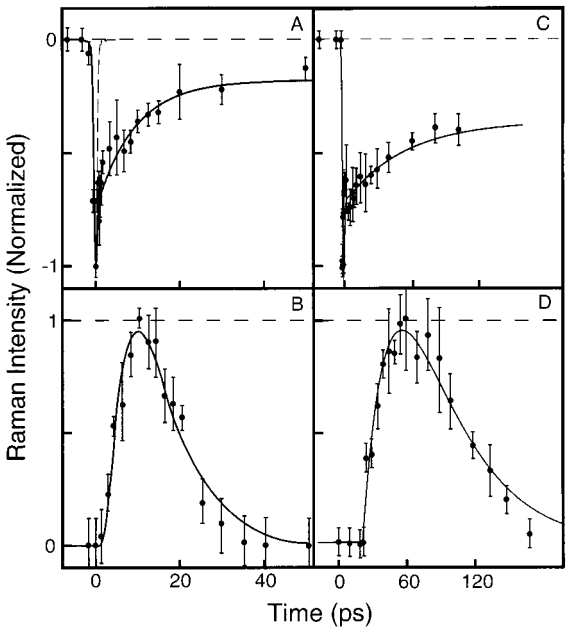

Figure 6. (A) Intensity of the aqueous OClO symmetric-stretch fundamental Stokes transition as a function of time. Best fit to the data by a sum of exponentials convolved with the instrument response (solid line) was obtained with time constants (with normalized amplitude in parentheses) of 0.15 ± 0.1 (0.65), 9.2 ± 3.5 (0.27), and 10 000 ps representing the long-time offset in intensity (0.08). (B) Intensity of the aqueous OClO symmetric stretch anti-Stokes fundamental transition as a function of time. Best fit to the data by a sum of two exponentials convolved with the instrument response (solid line) was obtained with an appearance time constant (with normalized amplitude in parentheses) of 5.2 ± 1.5 ps (0.5) and a decay time-constant of 9.2 ± 1.7 ps (0.5). (C) Temporal evolution for symmetric-stretch fundamental Stokes transition of OClO dissolved in acetonitrile. Best fit to the data by a sum of exponentials convolved with the instrument response (solid line) was obtained with time constants (with normalized amplitude in parentheses) of 0.15 ± 0.1 (0.8), 33.0 ± 8.1 (0.08), and 10 000 ps representing the long-time offset in intensity (0.12). (D) Intensity of the symmetric stretch anti-Stokes fundamental transition of OClO dissolved in acetonitrile as a function of time. Best fit to the data by a sum of two exponentials convolved with the instrument response (solid line) was obtained with an appearance time constant (with normalized amplitude in parentheses) of 33.7 ± 4.4 ps (0.5) and a decay time-constant of 36.7 ± 4.6 ps (0.5).

intensity confirms that the reformation of ground-state OClO is a dominant feature of solution-phase OClO photochemistry. Subpicosecond OClO reformation is observed in both solvents, suggesting that geminate-recombination rate is insensitive to the nature of the solvent. However, the efficiency of recombination is clearly solvent-dependent as evidenced by the decrease in the recombination quantum yield from 0.8 in water to 0.55 in acetonitrile. This behavior has been correlated with the extent of solvent self-association, where greater self-association provides for a stronger solvent cage and subsequently a greater geminate-recombination quantum yield. This hypothesis was tested in our TRRR studies of OClO dissolved in ethanol and 2,2,2-trifluoroethanol (TFE).[84] In this work, halogen substitution alters the solvent hydrogen-bonding strength and corresponds to the strength of the solvent cage. In this study, we found that the geminate-recombination quantum yield was significantly reduced in TFE, consistent with the propensity of this solvent to exist in monomeric form compared to the polymeric structures favored in ethanol.[85−87] Therefore, it appears that solvent self-association via hydrogen bonding is an important factor in defining geminate-recombination efficiencies. It should be noted that the geminate-recombination rate in TFE was not instrument-response limited, a result that was attributed to interaction of the photofragments with the solvent as evidenced by spectral evolution in the TRRR spectra.

The TRRR results in water and acetonitrile also demonstrate that the vibrational-relaxation dynamics of OClO are solvent dependent. Specifically, the agreement between the slower time recovery in Stokes intensity and the decay time of the anti-Stokes intensity demonstrates that intermolecular vibrational relaxation occurs with time constants of ∼9 and ∼35 ps in water and acetonitrile, respectively. The solvent dependence of the intermolecular vibrational relaxation rate has been assigned to two effects: solvent−solute vibrational mode overlap and/or intermolecular hydrogen bonding. In terms of mode overlap, low-frequency solute modes typically dominate intermolecular relaxation because the density of solvent accepting modes is greatest at lower frequency. In OClO, the lowest frequency coordinate is the bend having a frequency of 450 cm^{-1}, well matched to the librational band of water. However, the symmetric- (938 cm^{-1}) and asymmetric-stretch (1100 cm^{-1}) overlap well with the symmetric-stretch (918 cm^{-1}) and methyl-rock (1124 cm^{-1}) modes of acetonitrile. Because the vibrational relaxation rate is greater in water, the above comparisons suggest that the energy-dissipation rate is governed by dynamics involving the bend. The key test of this model is to monitor the vibrational relaxation dynamics of the bend, and such experiments are currently underway. Numerous studies have shown that solvent−solute hydrogen bonding can dramatically affect vibrational-relaxation rates.[88] The frequency of the OClO symmetric-stretch fundamental transition is sensitive to intermolecular hydrogen-bonding strength, changing from 945 cm^{-1} in water to 938 cm^{-1} in acetonitrile. In our TRRR studies of OClO dissolved in ethanol and TFE, this transition is observed at 940 cm^{-1} in both solvents, suggesting that the hydrogen bonding environment is similar.[84] Therefore, we might expect the vibrational-relaxation rate to be similar as well; however, the relaxation time increases from ∼30 ps in ethanol to ∼80 ps in TFE suggesting that hydrogen-bonding is not the dominant mechanism for vibrational energy deposition into the solvent. Furthermore, the similarity in vibrational-relaxation time constants for ethanol and acetonitrile clearly calls into question simple correlation between hydrogen bonding and the vibrational-relaxation rate. A detailed, microscopic-level description of OClO intermolecular vibrational relaxation awaits the application of theory. Toward this end, Benjamin and co-workers have performed molecular dynamics simulations of OClO in a variety of solvents, and excellent agreement between the computational and experimental relaxation rates is observed suggesting that such a description is close at hand.[89]

Cl Production following OClO Photoexcitation. The TRRR results presented above did not provide evidence for ClOO formation following OClO photoexcitation. However, this intermediate is formed in low-temperature matrixes, suggesting that ClOO production should also be appreciable in solution. To further explore the role of ClOO in OClO photochemistry, we performed TRRR studies using a probe wavelength of 260 nm.[45,90] The absorption cross section of ClOO is substantial at this wavelength;[36,91,92] therefore, these experiments provided the best opportunity to observe the formation and decay dynamics of this intermediate. The results obtained in our studies of aqueous OClO are presented in Figure 7A. At this probe wavelength, depletion in OClO scattering intensity is observed, and the extent of depletion decreases as the delay is increased. This behavior is entirely consistent with the geminate-

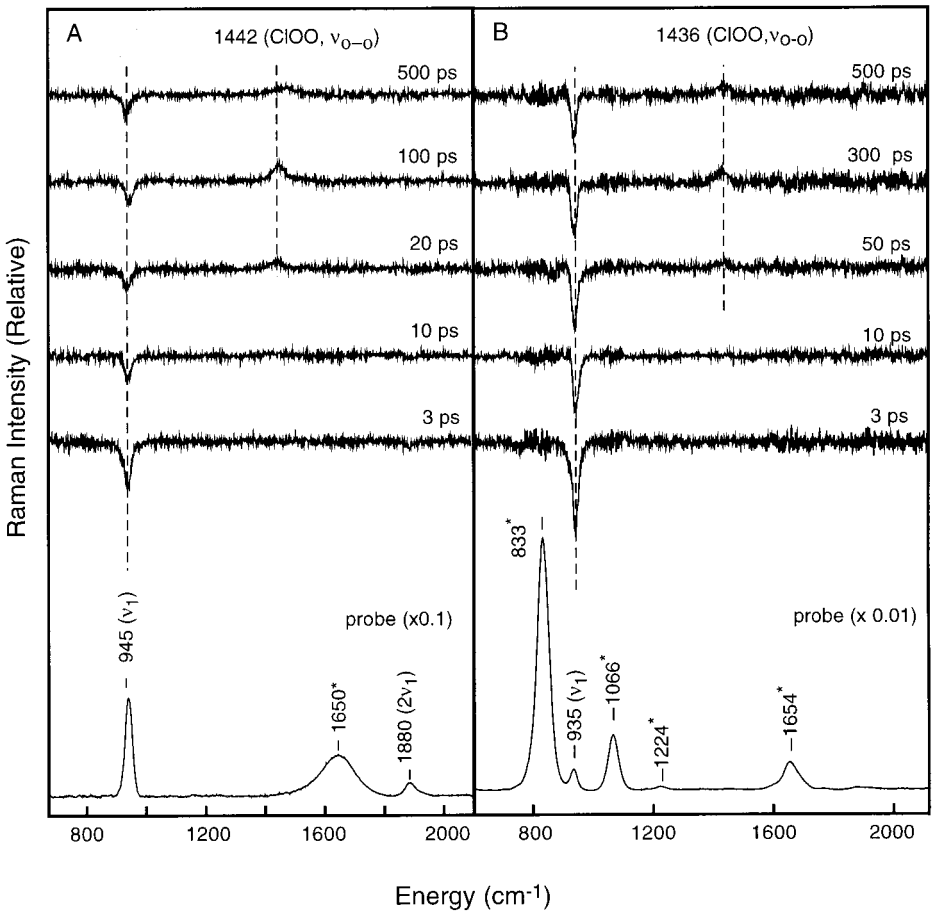

Figure 7. Time-resolved resonance Raman Stokes difference spectra of OClO dissolved in **(**A) water and (B) fluorotrichloromethane. Data were obtained using a 390 and 260 nm pump and probe beams, respectively. The temporal delay between the pump and the probe at which a given spectrum was obtained is indicated. The probe-only spectrum is presented at the bottom of each panel. Transitions marked with an asterisk in the probe-only spectra are due to the solvent.

recombination dynamics observed at 390 nm (see above). In contrast to our earlier TRRR studies, positive intensity at 1442 cm^{-1} is observed consistent with the appearance of ClOO.[32,33,93] The ClOO formation and decay kinetics were determined by plotting the intensity at 1442 cm^{-1} as a function of delay time (Figure 8A). This evolution was best modeled by two exponentials corresponding to appearance and decay time constants of 27.9 ± 4.5 and 398 ± 50 ps, respectively (Figure 8A). Both the appearance and decay time constants are in excellent agreement with corresponding values determined in femtosecond pump probe studies.[92]

We have also investigated OClO dissolved in fluorotrichloromethane (Freon-11) to determine if ClOO is produced via geminate recombination. This solvent was chosen for study because it is an aprotic solvent in which the absence of self-association via hydrogen bonding is anticipated to provide for a weaker solvent cage and a corresponding reduction in geminate recombination efficiency. Acetonitrile was employed for identical reasons in the studies presented above; however, this solvent could not be used here because of spectral overlap with ClOO. Figure 7B presents the TRRR results for OClO dissolved in Freon-11. Similar to the behavior observed in water, an initial depletion in OClO scattering intensity is observed. As the temporal delay is increased, the OClO depletion remains substantial suggesting that geminate recombination is less efficient in this solvent. Additional femtosecond pump−probe studies have demonstrated that the geminate-recombination quantum yield is only 0.3 ± 0.1 in Freon-11.[45] Studies were also performed in which the quantum yield for ClOO production in water and Freon-11 was determined, and this quantum yield was found to be equivalent in both solvents (0.02 ± 0.01). Therefore, the reduction in geminate-recombination efficiency does not result in a corresponding reduction in ClOO production. Finally, the kinetics of ClOO production in Freon-11 were determined through analysis of the ClOO scattered intensity as a function of time (Figure 8B), with best fit corresponding to appearance and decay times of 172 ± 30 and 864 ± 200 ps, respectively.

The similarity of the ClOO-production quantum yield between solvents in which geminate recombination efficiency is vastly different demonstrates that this intermediate is not produced by recombination of the primary photoproducts. Instead, we have proposed that the mechanism of ClOO production involves OClO photoisomerization. A similar mechanism was used to describe resonances observed in the REMPI spectra of Cl produced following OClO photoexcitation.[9,26] Furthermore, computational studies of the absorption and absolute resonance Raman cross section of ClOO indicate that the difference in appearance time constants is not due to solvent-dependence of the vibrational-relaxation rate but is instead due to a change in the rate of ground-state ClOO production.[45] These differences are presumably due to solvent-dependence of the ground- and excited-state energetics, but this hypothesis has yet to be tested. Finally, the solvent-dependence of ClOO decay has been assigned to greater stability of the Cl−water charge-transfer complex.

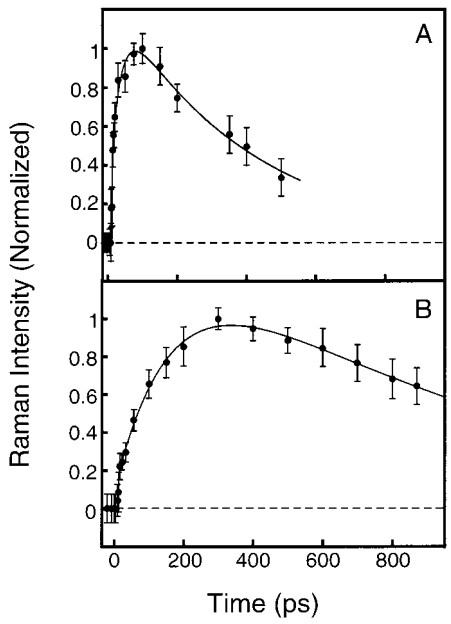

Figure 8. (A**)** Intensity of the ClOO transition at 1442 cm^{-1} in water as a function of time delay. The data were fit by a sum of two exponentials convolved with the instrument response resulting in appearance and decay time constants of 27.9 ± 4.5 and 398 ± 50 ps, respectively. In addition, inclusion of a 12.7 ± 1.5 ps dwell relative to zero time was necessary to reproduce the data. (B) Intensity of the same ClOO transition in Freon-11 as a function of time delay. The data were fit by a sum of two exponentials convolved with the instrument response resulting in appearance and decay time constants of 172 ± 30 and 864 ± 200 ps, respectively. In addition, inclusion of a 13 ± 0.4 ps dwell relative to zero time was necessary to reproduce the data.

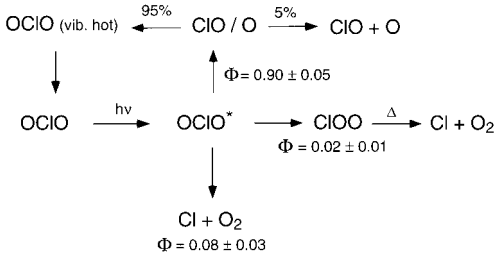

Figure 9. Current picture of aqueous OClO photochemistry. The quantum yields for various photochemical pathways are indicated.

Current Picture of Aqueous OClO Photochemistry

The TRRR and transient absorption studies outlined here have provided a detailed description of solution-phase OClO photochemistry as illustrated in Figure 9. As discussed in the Introduction, $\Phi_{Cl} = 0.1$ such that the dominant photochemical channel in solution is ClO and O production. These photoproducts undergo geminate recombination on the subpicosecond time scale resulting in the reformation of ground-state OClO. Once formed, OClO undergoes vibrational relaxation with a rate that is solvent dependent. The remainder of photoexcited OClO results in Cl production through a bifurcated process. ClOO production and decay represents the minor Cl production channel accounting for 20% of the overall Cl yield. The remainder of Cl is produced by a "direct" process, the details of which are largely unknown. Transient absorption studies have shown that this process involves an intermediate that decomposes to form Cl with a time constant of ~6 ps; however, the identity of this intermediate has yet to be established.

Given the picture presented in Figure 9, one may wonder what else there is to learn about OClO photochemistry? Although much progress has been made, there are many unresolved questions that need to be addressed. First, identification of the intermediate species responsible for the majority of Cl production is a key step in furthering our understanding of OClO photochemistry. Second, gas-phase studies have shown that the Cl production quantum yield is dependent on actinic wavelength,[17] and it is currently unclear if similar behavior occurs in condensed environments. Recent femtosecond pump−probe studies of aqueous OClO have suggested that the excited-state dynamics are dependent on the initial vibronic level produced.[94] This result strongly suggests that a change in the actinic wavelength will have a pronounced effect on photoproduct formation. In contrast, photochemical action spectra of OClO isolated in clusters suggest that the Cl production quantum yield is actinic-wavelength independent.[29] Therefore, the variation in OClO photochemistry with actinic-wavelength remains an important, yet unanswered question. Third, the TRRR studies presented were interpreted in terms of ClOO production via OClO photoisomerization. It is unclear if this behavior is unique to OClO or if photoisomerization is general feature of halooxide photochemistry. Toward this end, we have shown that ClOCl undergoes photoisomerization to produce ClClO on the <5 ns time scale.[95] However, the quantum yield and production kinetics of this isomer are still unknown. Finally, the work outlined here was performed with an eye toward the chemistry of halooxides in heterogeneous environments (i.e., interfaces). OClO orientation, the importance of geminate recombination, and the quantum yield for Cl production in such environments are all important issues that remain unexplored. The extension of this work to the interfacial domain will be a challenging and important avenue of study.

Acknowledgment. I acknowledge the vital contributions of my co-workers Bethany Barham, Anthony Esposito, Catherine Foster, Sophia Hayes, Matthew Philpott, and Carsten Thomsen (Aarhus University, Denmark). The National Science Foundation is acknowledged for their support of this work (CHE-9701717 and CHE-0091320). Acknowledgment is also made to the donors of the Petroleum Research Fund, administered by the American Chemical Society. P.J.R. is the recipient of a Dreyfus New-Faculty Award and an Alfred P. Sloan Fellowship and is a Cottrell Scholar of the Research Corporation.

References and Notes

(1) Farman, J. C.; Gardiner, B. G.; Shanklin, J. D. *Nature* **1985**, *315*, 207.

(2) Rowland, F. S. *Annu. Rev. Phys. Chem.* **1991**, *42*, 731.

(3) Sander, S. P., Friedl, R. R., Francisco, J. S., Barker, J. R., Ed.; *Progress and Problems in Atmospheric Chemistry*; World Scientific: Singapore, 1995.

(4) Molina, M. J.; Molina, L. T.; Golden, D. M. *J. Phys. Chem.* **1996**, *100*, 12888.

(5) Wayne, R. P. *The Chemistry of Atmospheres*, 2nd ed.; Oxford Science Publications: Oxford, U.K., 1991.

(6) Finlayson-Pitts, B. J.; Pitts, J. N. J. *Chemistry of the Upper and Lower Atomsphere*; Academic Press: San Diego, CA, 2000.

(7) Solomon, S.; Garcia, R. R.; Rowland, F. S.; Wuebbles, D. J. *Nature* **1986**, *321*, 755.

(8) Solomon, S.; Borrmann, S.; Garcia, R. R.; Portmann, R.; Thomason, L.; Poole, L. R.; Winker, D.; McCormick, M. P. *J. Geophys. Res.* **1997**, *102*, 21411.

(9) Vaida, V.; Solomon, S.; Richard, E. C.; Ruhl, E.; Jefferson, A. *Nature* **1989**, *342*, 405.

(10) Vaida, V.; Goudjil, K.; Simon, J. D.; Flanders, B. N. *J. Mol. Struct.* **1994**, *61*, 133.

(11) Vaida, V.; Simon, J. D. *Science* **1995**, *268*, 1443.

(12) Reid, P. J. *Acc. Chem Res.* **2001**, *134*, 691.

(13) Sessler, J.; Chipperfield, M. P.; Pyle, J. A.; Toumi, R. *Geophys. Res. Lett.* **1995**, *22*, 687.

(14) Miller, H. L.; Sanders, R. W.; Solomon, S. *J. Geophys. Res.* **1999**, *104*, 18769.
(15) Wagner, T.; Carsten, L.; Pfeilsticker, K.; Platt, U. *J. Geophys. Res.* **2001**, *106*, 4971.
(16) Davis, H. F.; Lee, Y. T. *J. Phys. Chem.* **1992**, *96*, 5681.
(17) Davis, H. F.; Lee, Y. T. *J. Chem. Phys.* **1996**, *105*, 8142.
(18) Bishenden, E.; Haddock, J.; Donaldson, D. J. *J. Phys. Chem.* **1991**, *95*, 2113.
(19) Bishenden, E.; Donaldson, D. J. *J. Chem. Phys.* **1993**, *99*, 3129.
(20) Bishenden, E.; Donaldson, D. J. *J. Chem. Phys.* **1994**, *101*, 9565.
(21) Baumert, T.; Herek, J. L.; Zewail, A. H. *J. Chem. Phys.* **1993**, *99*, 4430.
(22) Delmdahl, R. F.; Bakker, D. L. G.; Parker, D. H. *J. Chem. Phys.* **2000**, *112*, 5298.
(23) Delmdahl, R. F.; Ullrich, S.; Gericke, K.-H. *J. Phys. Chem. A* **1998**, *102*, 7680.
(24) Delmdahl, R. F.; Baumgartel, S.; Gericke, K.-H. *J. Chem. Phys.* **1996**, *194*, 2883.
(25) Roth, M.; Maul, C.; Gericke, K. H. *J. Chem. Phys.* **1997**, *107*, 10582.
(26) Ruhl, E.; Jefferson, A.; Vaida, V. *J. Phys. Chem.* **1990**, *94*, 2990.
(27) Flesch, R.; Wassermann, B.; Rothmund, B.; Ruhl, E. *J. Phys. Chem.* **1994**, *98*, 6263.
(28) Lawrence, W. G.; Clemitshaw, K. C.; Apkarian, V. A. *J. Geophys. Res.* **1990**, *95*, 18591.
(29) Kreher, C. J.; Carter, R. T.; Huber, J. R. *J. Chem. Phys.* **1999**, *110*, 3309.
(30) Kreher, C. J.; Carter, R. T.; Huber, J. R. *Chem. Phys. Lett.* **1998**, *286*, 389.
(31) Furlan, A.; Scheld, H. A.; Huber, J. R. *J. Chem. Phys.* **1997**, *106*, 6538.
(32) Arkell, A.; Schwager, I. *J. Am. Chem. Soc.* **1967**, *89*, 5999.
(33) Mueller, H. S. P.; Willner, H. *J. Phys. Chem.* **1993**, *97*, 10589.
(34) Lanzendorf, E. J.; Kummel, A. C. *Geophys. Res. Lett.* **1996**, *23*, 1251.
(35) Adrian, F. J.; Bohandy, J.; Kim, B. F. *J. Chem. Phys.* **1986**, *85*, 2692.
(36) Pursell, C. J.; Conyers, J.; Alapat, P.; Parveen, R. *J. Phys. Chem.* **1995**, *99*, 10433.
(37) Dunn, R. C.; Simon, J. D. *J. Am. Chem. Soc.* **1992**, *114*, 4856.
(38) Dunn, R. C.; Flanders, B. N.; Simon, J. D. *J. Phys. Chem.* **1995**, *99*, 7360.
(39) Thøgersen, J.; Thomsen, C. L.; Poulsen, J. A.; Keiding, S. R. *J. Phys. Chem. A* **1998**, *102*, 4186.
(40) Poulsen, J. A.; Thomsen, C. L.; Keiding, S. R.; Thøgersen, J. *J. Chem. Phys.* **1998**, *108*, 8461.
(41) Thøgersen, J.; Jepsen, P. U.; Thomsen, C. L.; Poulsen, J. A.; Byberg, J. R.; Keiding, S. R. *J. Phys. Chem.* **1997**, *101*, 3317.
(42) Philpott, M. J.; Charalambous, S.; Reid, P. J. *Chem. Phys. Lett.* **1997**, *281*, 1.
(43) Bursa, M. A.; Perissinotti, L. J.; Churio, M. S.; Colussi, A. J. *J. Photochem. Photobio. A: Chem.* **1996**, *101*, 105.
(44) Thomson, C. L.; Philpott, M. P.; Hayes, S. C.; Reid, P. J. *J. Chem. Phys.* **2000**, *112*, 505.
(45) Hayes, S. C.; Thomsen, S. C.; Reid, P. J. *J. Chem. Phys.* **2001**, *115*, 11228.
(46) Graham, J. D.; Roberts, J. T.; Brown, L. A.; Vaida, V. *J. Phys. Chem.* **1996**, *100*, 3115.
(47) Brown, L. A.; Vaida, V.; Hanson, D. R.; Graham, J. D.; Roberts, J. T. *J. Phys. Chem.* **1996**, *100*, 3121.
(48) Coon, J. B. *Phys. Rev.* **1940**, *58*, 926.
(49) Coon, J. B. *J. Chem. Phys.* **1946**, *14*, 665.
(50) Mulliken, R. A. *Can. J. Chem.* **1958**, *36*, 10.
(51) Lawless, M. K.; Reid, P. J.; Mathies, R. A. In *Analysis of Condensed Phase Photochemical Reaction Mechanisms with Resonance Raman Spectroscopy*; Simon, J. D., Ed.; Kluwer: Amsterdam, The Netherlands, 1994; pp 267−287.
(52) Richard, E. C.; Vaida, V. *J. Chem. Phys.* **1991**, *94*, 153.
(53) Richard, E. C.; Vaida, V. *J. Chem. Phys.* **1991**, *94*, 163.
(54) Brand, J. C. D.; Redding, R. W.; Richardson, A. W. *J. Mol. Spectrosc.* **1970**, *34*, 399.
(55) Peterson, K. A.; Werner, H.-J. *J. Chem. Phys.* **1992**, *96*, 8948.
(56) Peterson, K. A.; Werner, H− J. *J. Chem. Phys.* **1996**, *105*, 9823.
(57) Peterson, K. A. *J. Chem. Phys.* **1998**, *109*, 8864.
(58) Xie, D.; Guo, H. *Chem. Phys. Lett.* **1999**, *307*, 109.
(59) Esposito, A.; Foster, C.; Beckman, R.; Reid, P. J. *J. Phys. Chem. A* **1997**, *101*, 5309.
(60) Reid, P. J.; Esposito, A. P.; Foster, C. E.; Beckman, R. A. *J. Chem. Phys.* **1997**, *107*, 8262.
(61) Foster, C. E.; Reid, P. J. *J. Phys. Chem. A* **1998**, *102*, 3541.
(62) Esposito, A. P.; Stedl, T.; Jonsson, H.; Reid, P. J.; Peterson, K. A. *J. Phys. Chem. A.* **1999**, *103*, 1748.
(63) Foster, C. E.; Barham, B. P.; Reid, P. J. *J. Chem. Phys* **2001**, *114*, 4892.
(64) Myers, A. B.; Mathies, R. A. In *Resonance Raman Intensities: A Probe of Excited-State Structure and Dynamics*; Spiro, T. G., Ed.; John Wiley & Sons: New York, 1987; Vol. 2, pp 1−58.
(65) Myers, A. B. *Chem. Phys.* **1994**, *180*, 215.
(66) Myers, A. B. *J. Raman Spectrosc.* **1997**, *28*, 389.
(67) Lee, S.-Y.; Heller, E. J. *J. Chem. Phys.* **1979**, *71*, 4777.
(68) Tannor, D. J.; Heller, E. J. *J. Chem. Phys.* **1982**, *77*, 202.
(69) Myers, A. B. *Annu. Rev. Phys. Chem.* **1998**, *49*, 267.
(70) Dunn, R. C.; Anderson, J. L.; Foote, C. S.; Simon, J. D. *J. Am. Chem. Soc.* **1993**, *115*, 5307.
(71) Hayes, S. C.; Cooksey, C. C.; Wallace, P. M.; Reid, P. J. *J. Phys. Chem. A* **2001**, *105*, 9819.
(72) Berg, M. *Chem. Phys. Lett.* **1994**, *228*, 317.
(73) Berg, M. *J. Phys. Chem. A* **1998**, *102*, 17.
(74) Berg, M. A. *J. Chem. Phys.* **1999**, *110*, 8577.
(75) Aherne, D.; Tran, V.; Schwartz, B. J. *J. Phys. Chem. B* **2000**, *104*, 5382.
(76) Ladanyi, B. M.; Stratt, R. M. *J. Phys. Chem.* **1995**, *99*, 2502.
(77) Dunn, R. C.; Richard, E. C.; Vaida, V.; Simon, J. D. *J. Phys. Chem.* **1991**, *95*, 6060.
(78) Chang, Y. J.; Simon, J. D. *J. Phys. Chem.* **1996**, *100*, 6406.
(79) Philpott, M. J.; Charalambous, S.; Reid, P. J. *Chem. Phys.* **1998**, *236*, 207.
(80) Hayes, S. C.; Philpott, M. J.; Reid, P. J. *J. Chem. Phys.* **1998**, *109*, 2596.
(81) Hayes, S. C.; Philpott, M. P.; Mayer, S. G.; Reid, P. J. *J. Phys. Chem. A* **1999**, *103*, 5534.
(82) Schwartz, B. J.; King, J. C.; Harris, C. B. In *Analysis of Condensed Phase Photochemical Reaction Mechanisms with Resonance Raman Spectroscopy*; Simon, J. D., Ed.; Kluwer: Dordrecht, The Netherlands, 1994.
(83) Walhout, P. K.; Alfano, J. C.; Thakur, K. A. M.; Barbara, P. F. *J. Phys. Chem.* **1995**, *99*, 7568.
(84) Philpott, M. J.; Hayes, S. C.; Thomsen, C. L.; Reid, P. J. *Chem. Phys.* **2001**, *263*, 389.
(85) Kivinen, A.; Murto, J. *Suom. Kemistil.* **1967**, *40*, 6.
(86) Krueger, P. J.; Mettee, H. D. *Can. J. Chem.* **1964**, *42*, 340.
(87) Blainey, P. C.; Reid, P. J. *Spectrosc. Acta A* **2001**, in press.
(88) Owrutsky, J. C.; Raftery, D.; Hochstrasser, R. M. *Annu. Rev. Phys. Chem.* **1994**, *45*, 519.
(89) Benjamin, I. Private communication.
(90) Thomsen, C. L.; Philpott, M. P.; Hayes, S. C.; Reid, P. J. *J. Chem. Phys.* **2000**, *112*, 505.
(91) Mauldin, R. L., III; Burkholder, J. B.; Ravishankara, A. R. *J. Phys. Chem.* **1992**, *96*, 2582.
(92) Thomsen, C. L.; Reid, P. J.; Keiding, S. R. *J. Am. Chem. Soc.* **2000**, *122*, 12795.
(93) Rochkind, M. M.; Pimentel, G. C. *J. Chem. Phys.* **1967**, *46*, 4481.
(94) Fidder, H.; Tschirschwitz, F.; Duhr, O.; Nibbering, E. T. J. *J. Chem. Phys.* **2001**, *114*, 6781.
(95) Esposito, A. P.; Reid, P. J.; Rousslang, K. W. *J. Photochem. Photobiol. A: Chem.* **1999**, *129*, 9.